Highly coordinated mechanical motion mediated by the microtubule cytoskeleton is a pivotal element of *de-novo* symmetry breaking in *hydra* spheroids

Heike Sander[a], Aravind Pasula[a], Mathias Sander[a], Varun Giri[a], Emmanuel Terriac[b], Franziska Lautenschlaeger[ab] and Albrecht Ott[a]

The establishment of polarity in cells and tissues is one of the first steps in multicellular development. The 'eternal embryo' *hydra* can completely regenerate from a disorganised cell cluster or a small fragment of tissue of about $10,000$ cells. During regeneration, the cells first form a hollow cell spheroid, which then undergoes *de-novo* symmetry breaking to irreversibly polarise. Here, we address the symmetry-related shape changes. Prior to axis establishment, the spherical aggregates of regenerating cells show highly coordinated mechanical oscillations on several timescales that are isotropic in space. There are transient periods of fluctuations in defined arbitrary directions, until these undergo a clearly identified irreversible transition to directed fluctuations along the future main axis of the regenerating *hydra*. Stabilised cytosolic actin structures disappear during the *de-novo* polarisation, while polymerised microtubules remain. Drugs that depolymerise actin filaments accelerate the symmetry breaking process, while drug-stabilised actin filaments prevent it. Nocodazole-depolymerised microtubules prevent symmetry breaking, but it can be rescued by the microtubule-stabilising drug paclitaxel at concentrations where microtubular structures start to reappear. We discuss the possibility that these mechanical fluctuations induce the orientation of the microtubules, which contribute to β-catenin nuclear translocation, to increase the organiser-forming-potential of the cells. Our data suggest that in regenerating *hydra* spheroids, the biomechanical shape fluctuations are an integral part of the cooperative polarisation of the self-organising *hydra*, during which microtubules play a pivotal role.

1 Introduction

The freshwater polyp *hydra* consists of a cell bilayer with a radially symmetric body, with one mouth opening. Hydra has astonishing capabilities for regrowth of lost body parts. Dissociation into single cells, mixing and random reaggration gives rise to a new hydra that forms from the disorganized heap. The first step towards regrowth from such a random cellular aggregate is the formation of an isotropic, hollow spheroid of about $10,000$ *hydra* cells. These then polarise and transform into fully functional *hydra*[1], albeit smaller than the adult consisting of about 100.000 cells. Hydra is considered to be a model organism for the study of symmetry breaking in developing tissues[2,3].

Suggested mechanisms for establishment of polarity in tissues include reaction-diffusion systems, asymmetric cell division, cell migration, cell sorting and pre-patterning. However, these multiple mechanisms cannot account for all of the known experimental observations[4].

Wnt and its associated pathways are involved in body patterning in cnidaria and bilateria. It is believed that the common ancestor of these clades developed a set of *Wnt* genes that promoted the patterning of the ancient body axis[5]. In *hydra* spheroids *de-novo* head formation occurs via activation of the canonical Wnt pathway[6–8]. The role of this pathway in the set-up of the head organiser and in maintenance of the body plan of *hydra* has been investigated in great detail[5,6,9–12].

[a] *Universität des Saarlandes, Biologische Experimentalphysik, Campus B2.1, 66123 Saarbrücken, Germany. Tel: +49681 302 68555, corresponding author e-mail: albrecht.ott@physik.uni-saarland.de*

[b] *INM - Leibniz-Institut für Neue Materialien gGmbH, Campus D2.2, 66123 Saarbrücken, Germany. Tel: +49681 9300 460, e-mail: F.Lautenschlaeger@physik.uni-saarland.de*

However, how and why the Wnt head-organising centre is initially established at a certain location within a regenerating hydra spheroid is unknown. No external stimuli have been identified, as in *Drosophila*[13], nor have the corresponding molecular players of suggested reaction-diffusion mechanisms, although the *dickkopf* gene has been suggested to be an antagonist here[5].

In the absence of superordinate structures or external polarising stimuli, symmetry breaking in tissues requires concerted actions among the cells. Intercellular nearest-neighbour communication is sufficient to generate asymmetry[4,14,15]. *Hydra* axis establishment occurs at the moment where the gene expression pattern of the *ks1* gene (which is a marker of head-forming potential[16]), expressed on the surface of the spheroid, tends to scale in shape and size[17]. Gamba *et al.* showed theoretically that nearest-neighbour-coupled, fluctuation-driven, avalanche-like propagation precisely and quantitatively reproduces the observed gene expression patterns in space and time, whereby the only free parameter of the model is the probability of information loss when transmission between neighbouring cells occurs. Moreover, should a huge avalanche be locked to create asymmetry, the head orientation in a weak temperature gradient (*i.e.*, below 1°C across the spheroid) will depend not only on gradient direction, but also on gradient amplitude, in excellent agreement with experimental data[18]. This result strongly supports the idea that information exchange is limited to neighbouring cells that tend to follow the stimulation from their individual environment, in conjunction with strong fluctuations in gene expression. This is opposed to the concept of the formation of a pre-patterned and controlled, spheroid-spanning morphogen gradient[19].

Fuetterer *et al.* described cyclic osmotic inflation and subsequent breakage of regenerating hydra spheroids that showed ir-

reversible transition from symmetric to asymmetric inflation[20]. Based on the observation that the level of biochemical or mechanical slowdown is in quantitative agreement with the observed delay in organiser formation, Soriano *et al.* suggested that this cyclic inflation is the driving clock of the symmetry-breaking process. They suggested a mechanically driven Turing model that leads to asymmetry[21]. This idea was taken up by Mercker *et al.*, who postulated a mechanobiochemical feedback loop between tissue stretching, resistance to lateral tissue stretching, and the behaviour of a head-defining morphogen[22]. However, the exact role of the mechanical behaviour and its connection to symmetry breaking remains unclear[23].

The eukaryotic cytoskeleton is a mechanically active structure, of great importance for cell signaling. It is a universal and evolutionarily old cellular component that predates the emergence of complex body structures[24]. Tubulins form polarised structures. They share a common ancestor with bacterial tubulin homologues[25]. The integrins were the first extracellular matrix proteins. They briefly predated the appearance of the *holozoa*[26], as for the collagens and the emergence of *metazoa*[27]. *Hydra* contain large supercellular contractile actin structures, which are known as myonemes[28]. Actin fibres have been shown to be responsible for the maintenance of polarity in *hydra* regeneration from tissue fragments that are large enough not to undergo *de-novo* axis definition[29].

Mechanotransduction and the role of cytoskeletal elements in the establishment of polarity have been detailed for other model organisms. The cytoskeleton is involved in the polarisation process of zebrafish *Danio rerio* and *Drosophila*[30]. Tissue elongation of *Drosophila* follicle cells requires oscillating contractions of a basal actomyosin network[31]. The embryonic elongation of *Caenorhabditis elegans* also involves myosin II[32]. Mechanotransduction transmitted by the cytoskeleton can have a major role in gastrulation[33,34]. Mechanical fluctuations at a subcellular level can affect the polarisation of individual cells during development[35–37].

Here we investigated shape-symmetry breaking and the role of the cytoskeletal components in *de-novo* axis establishment of regenerating *hydra* spheroids.

2 Results

Shape changes in regenerating *hydra* spheroids - identification of symmetry breaking

Fragments cut out of the *hydra* body column fold inwards until hollow spheroids emerge, made up of a cell bilayer. Sufficiently small fragments lose their former body axis[21]. For the present study, these hollow spheroids were kept in drops of buffer that were hanging from the lids of petri dishes.

The shapes of the regenerating small fragments were recorded as a function of time using a microscope equipped with a digital camera.

During the initial oscillations of the spheroids, cells were disgorged at each deflation, which resulted in reductions in the diameter. For all of the initial diameters studied (*i.e.*, $0.2-0.5$mm), the body axis only emerged after the size reduction (Fig. 1 Centre). The mean diameter of the relaxed spheroid was 0.2 ± 0.01mm ($n=15$ *hydra* spheroids; Supplementary Information figure S1)). The Pearson correlation coefficients revealed a linear relationship between the time required for the size adjustment and the magnitude of the size change (correlation coefficient: $0.96\pm 2\cdot 10^{-8}$; Supplementary Information figure S2). The Spearman correlation coefficient revealed that the time required for the size adjustment did not correlate with the length of the following time interval until axis establishment (Spearman correlation coefficient: -0.01, significance 0.97, $n=15$ *hydra* spheroids; Supplementary Information figure S3).

From the images obtained, the volumes of the spheroids were approximated by fitting an ellipse to the mid-plane sectional image and computing the volumes of the rotational ellipsoids (Fig. 1a). Most of the regeneration patterns initially showed large oscillations in spheroid volume that decreased in amplitude[20], to eventually stabilise.

The angle of the major axis with respect to the image frame enabled us to follow the time course of the spatial direction of the hydra ellipsoids (Fig. 1b). Before symmetry breaking, on a timescale of minutes, phases where the angle remained stable in space alternated with phases where the angle varied rapidly (Fig. 1b, right panel). This variation was due to successive elongation of the spheroid in different spatial directions. The slow change in the angle, after the symmetry breaking, seen in figure 1b corresponds to a slow rotation of the spheroid in the hanging drop.

We took the circularity as the ratio of the minor to major axes of the ellipsoid, as described in figure 1c. A ratio of 1.0 corresponds to a perfect sphere, while 0 to a straight line. Irreversible axis establishment, *i.e.*, symmetry breaking, was identified by the irreversible transition to a stable direction of the axis in space, accompanied by the onset of an irreversible decrease in the circularity.

Application of a mechanical stimulus

To apply a mechanical stimulus during the symmetry-breaking process, the spheroids were held in place using a micropipette (see Fig. 2, inset). The internal suction pressure of the pipette was maintained constant during the regeneration process. There were no apparent changes regarding the regeneration time. The stimulus from the pipette led to the heads emerging within an annular zone around the pipette tip, *i.e.*, at an average angle smaller than perpendicular to the axis of the pipette (Fig. 2).

Actin structure under confocal microscopy

In adult *hydra*, the actin myonemes are arranged into two orthogonal layers, with the inner layer surrounding the *hydra* perpendicular to the body axis, and the outer layer spanning the *hydra* along the direction of the body axis (Fig. 3). After rounding up, in the early spheroid cortical actin and cytosolic actin stress fibres can be observed (Fig. 4). Both the actin myonemes and stress fibres disappear within 30min in case the emerging spheroids are sufficiently small (diameter $< 450\mu$m; figure 4). The actin myonemes and cytosolic structures are reestablished only after the shape-symmetry breaking, 18h to 24h after the cutting of the *hydra*.

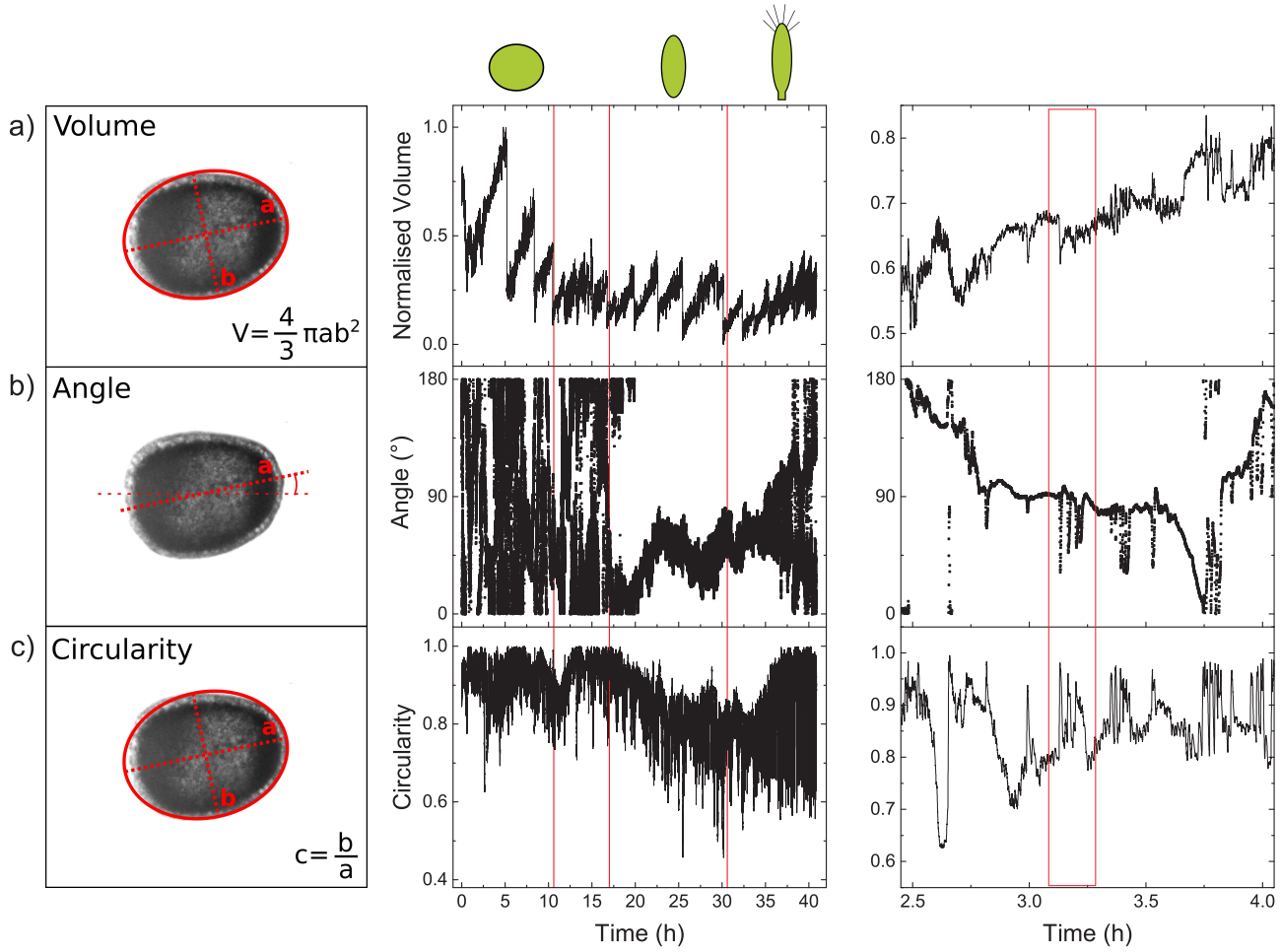

Fig. 1 *Hydra* regeneration. Definition of the parameters (left) and their evolution as a function of time (centre) for a typical *hydra* regeneration (~ 2 days). The pictograms (top) illustrate the overall shapes of the regenerating *hydra* during different periods of regeneration. **Left:** Images of regenerating *hydra* cell spheres were fitted to an ellipse. **(a) Volume**, as determined from the ellipsoid of rotation. **(b) Angle**, between the major axis of the ellipsoid and the reference axis (image frame). **(c) Circularity**, the ratio of the minor to the major axis of the ellipsoid, where a value of 1.0 corresponds to a sphere, and 0 to a straight line. **Centre:** The three parameters, Volume (normalised, arbitrary units), Angle (degrees), and Circularity as functions of time. The first red line indicates the end of the size-reduction period. In all studied cases shape symmetry breaking was only observed beyond this point. The second line indicates the transition from a situation where the sphere fluctuates by elongating in different random directions, to a situation where the axis remains irreversibly fixed for the sphere. This point defines the shape-symmetry breaking instant. The slow change in the angle after this point is due to slow rotation of the elongated cell sphere in the hanging drop. The circularity starts to decrease almost at the same moment as the angle stabilises, which shows that the ellipsoidal deformation becomes more and more pronounced. The third red line indicates the moment where the *hydra* tentacles appear. After this point, the *hydra* moves actively and an ellipsoid does not fit the observed shape any more. The values of volume, angle and circularity start to increase, or scatter, but this does not represent quantitative changes. **Right:** Oscillations in the volume, angle, and circularity at a time scale of minutes to hours. A representative example of the correlations between the volume, angle and circularity oscillations is highlighted by the red frame.

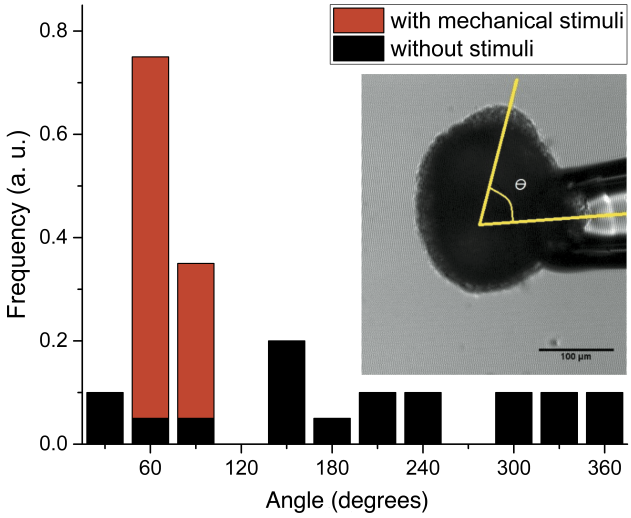

Fig. 2 The mechanical stimulus of the micropipette suction determines the axis orientation. The distribution of the angles of *hydra* axis formation with respect to the pipette axis ('with mechanical stimuli') and in the absence of aspiration ('without stimuli'). **Inset:** A *hydra* spheroid fixed by micropipette aspiration. The tissue was aspirated into the pipette using 60μm diameter. We observed that the *hydra* axis developed in a plane oriented $40-70^\circ$ to the pipette as indicated by the yellow lines.

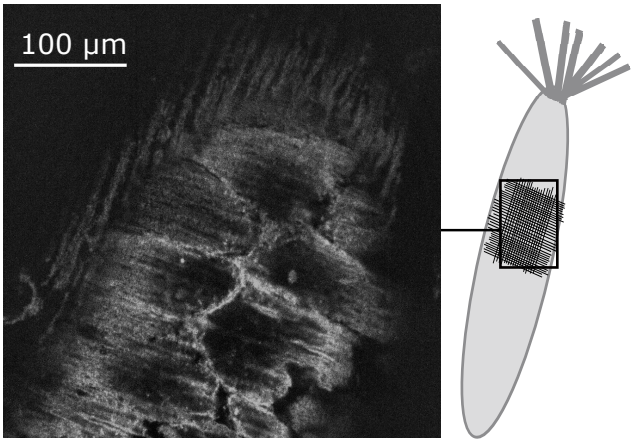

Fig. 3 Actin myonemes in adult *hydra* as observed by confocal microscopy. The cortical actin and the actin myonemes were stained using rhodamin-phalloidin. The orthogonal layers of the actin myonemes can be distiguished.

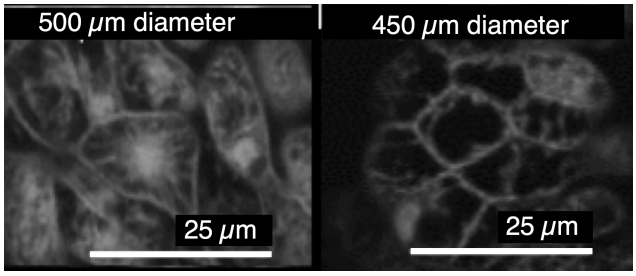

Fig. 4 Loss of intracellular actin structures in transgenic live actin-GFP *hydra* spheroids observed by confocal microscopy. Representative images of the ectodermal layer taken 60min after a fragment was cut from a hydra for regeneration. **Left panel:** *Hydra* spheroid with an initial diameter of $\approx 500\mu$m. The cellular actin structures are visible as a network. This spheroid showed asymmetric fluctuations in a fixed direction from the beginning. **Right panel:** Smaller spheroid with an initial diameter of $\approx 450\mu$m. The intracellular structures have disappeared, but actin structures remain visible within the cellular cortex. These spheroids underwent symmetry breaking as described in figure 1.

Influence of cytoskeleton-directed drugs on *hydra* spheroid motion

We investigated actin structure-modifying drugs for their impact on the shape development of *hydra* spheroids, including phalloidin (actin stabiliser), Y-27632 (inhibitor of p160 ROCK and actin contractility), and SMIFH2 (inhibitor of Formin and *de-novo* stress fibre formation[38,39]), as well as the influence of the microtubule-modifying drugs nocodazole (depolymerising) and paclitaxel (stabilising). Their influence on the shape evolution of the spheroids is shown in figures 5 (actin-modifying drugs) and 6 (microtubule-modifying drugs). Nocodazole-treated spheroids did not develop at concentrations as low as 0.1μM nocodazole ($n = 15$). However, the development was rescued by addition of 0.1μM paclitaxel 24h later (12 out of 15 spheroids) (Fig. 7). Microtubule staining revealed that the rescued development correlated with increased presence of polymerised microtubules, including supercellular structures emerging after 24h, that is, before axis formation (Fig. 8).

In figure 1 (right panel) fluctuations of volume, angle and circularity appear correlated. The cross-correlations among these parameters as a function of time were determined after subtraction of the underlying linear increases in the 'sawtooth' volume oscillations (Supplementary Information figure S4 for details on the subtraction). The rhythmic oscillations in the volume, from the start until axis establishment, on a time scale of minutes correlated with the oscillations of the orientation of the major axis (correlation coefficient, volume and angle: 0.9 ± 0.0306, $n = 17$ *hydra* spheroids). The time evolution of the angle, from the beginning of the first inflation until appearance of the tentacles, correlated with the circularity (correlation coefficient, angle and minor/major axis ratio: 0.83 ± 0.19, $n = 17$ *hydra* spheroids). In figure 1 (right panel,b) periods of quiescence can be distinguished from periods where fluctuations of the angle occur. We chose a minimum threshold amplitude to define fluctuations, and plotted the summed probability of periods of quiescence as a function of the duration of the periods of quiescence (see Image analy-

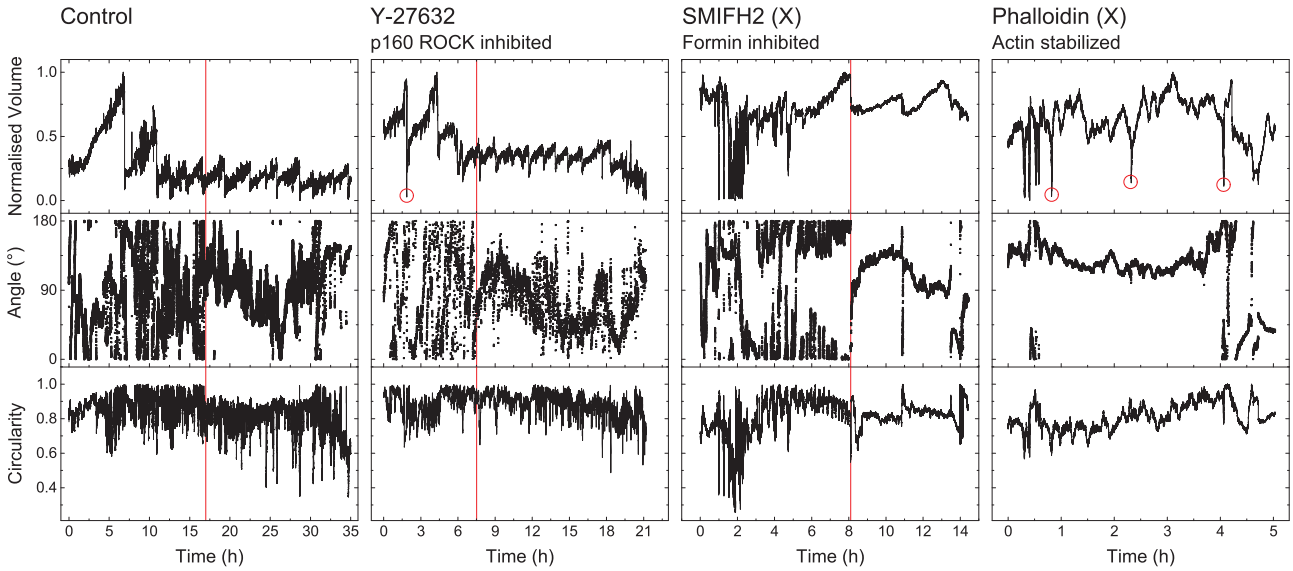

Fig. 5 Normalised volume, angle and circularity of regenerating *hydra* spheres under treatments with actin-modifying drugs as a function of time. Unsuccessful regenerations (in the cases of SMIFH2 and Phalloidin treatment) are indicated by (X). **Control:** Untreated spheroid. **Y-27632** (ROCK inhibitor): Inhibition of actin contractility. The initial volume inflations showed long, downward-pointing peaks that were not present in the control (red circles). The symmetry breaking appeared much earlier (red line), ~ 7.5h versus ~ 17h in control. However, the axis angle appeared more scattered compared to the control, which indicated more pronounced fluctuations of the shape. **SMIFH2** (Formin inhibitor): Inhibition of *de-novo* stress fibre formation. The sudden stabilisation of the spatial orientation of the major axis remained visible (red line), however the regenerating *hydra* did not elongate (the circularity did not decrease). The spheroids failed to regenerate. **Phalloidin**: Stabilisation of actin structures. The large volume sawtooth oscillations seen in the control did not occur. Downward pointing peaks of the volume appeared (indicated by circles). The axis angle remained stable in space during the entire observation time, which indicated that the initial symmetry was not lost. At the same time, the cell balls rounded up, as can be seen from the increase in circularity. Eventually the spheres started to disintegrate.

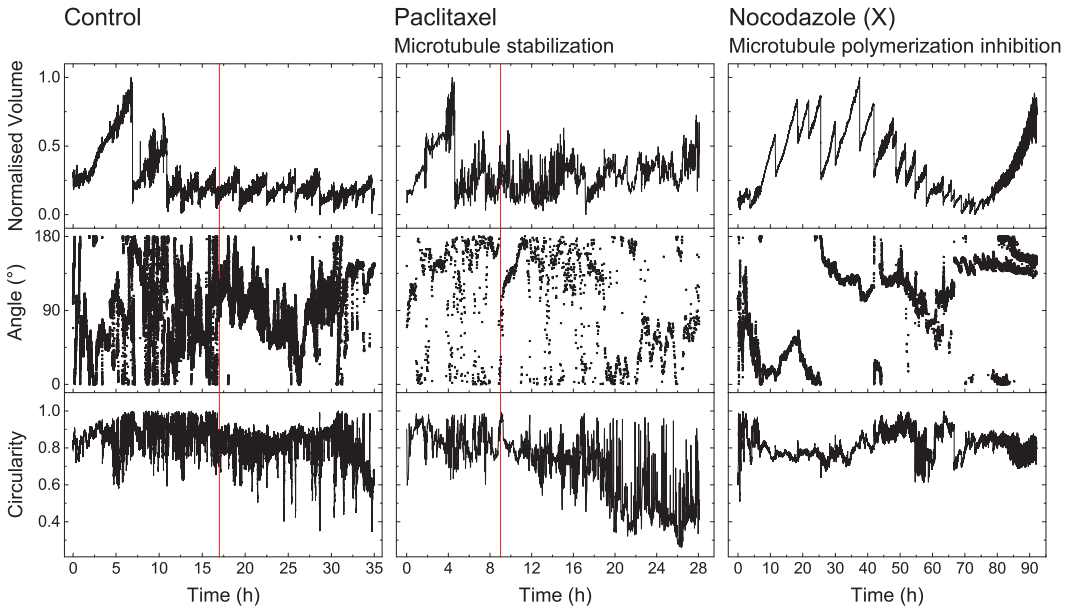

Fig. 6 Normalised volume, angle and circularity of regenerating hydra spheroids as a function of time and treatment with microtubule-modifying drugs. Unsuccessful regeneration (in the case of Nocodazole treatment) is indicated by an (X). **Control:** Untreated spheroid. **Paclitaxel:** Stabilisation of microtubule polymerisation. The red line indicates the moment where the sphere started to elongate irreversibly, and the direction of the axis was established. Although the direction of the axis showed more pronounced fluctuations in time than the control, the *hydra* regenerated successfully. **Nocodazole**: Inhibition of microtubule polymerisation. The axis direction and circularity during the first 24h suggest that the symmetry of the spheroid remained broken from the beginning. After 24h, the aggregate started to shrink and then disintegrated as reflected by the increase in volume beginning ~ 75h.

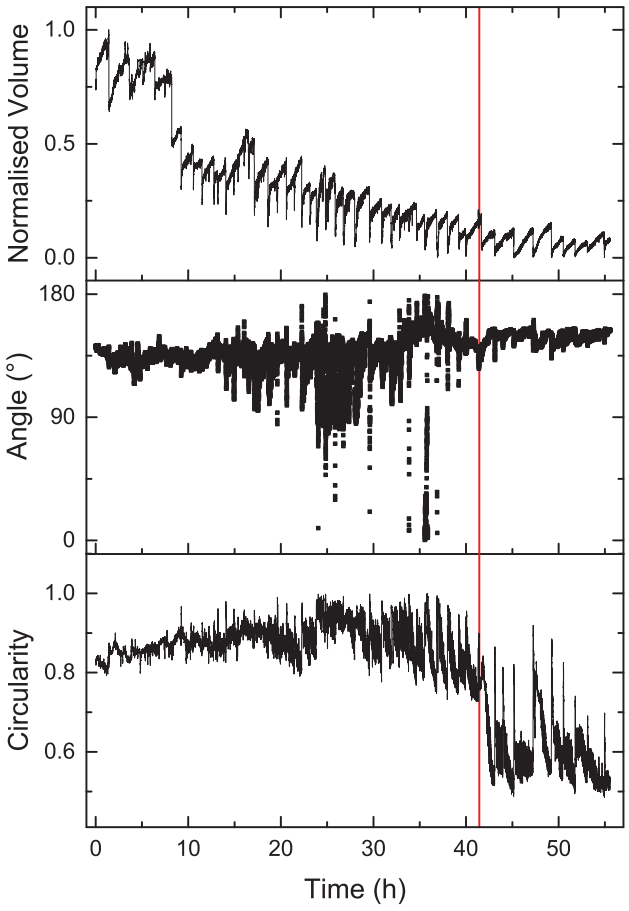

Fig. 7 Shape changes of a *hydra* spheroid treated for 24h with 0.1μM nocodazole, then exposed to 0.1μM paclitaxel. The *hydra* spheroid established an axis only after about ~ 41h (red line) counted from paclitaxel addition, that is, 65h after spheroid formation. Nocodazole-treated spheroids without paclitaxel treatment did not show signs of developing asymmetry and disintegrated (Supplementary Information figure S5)).

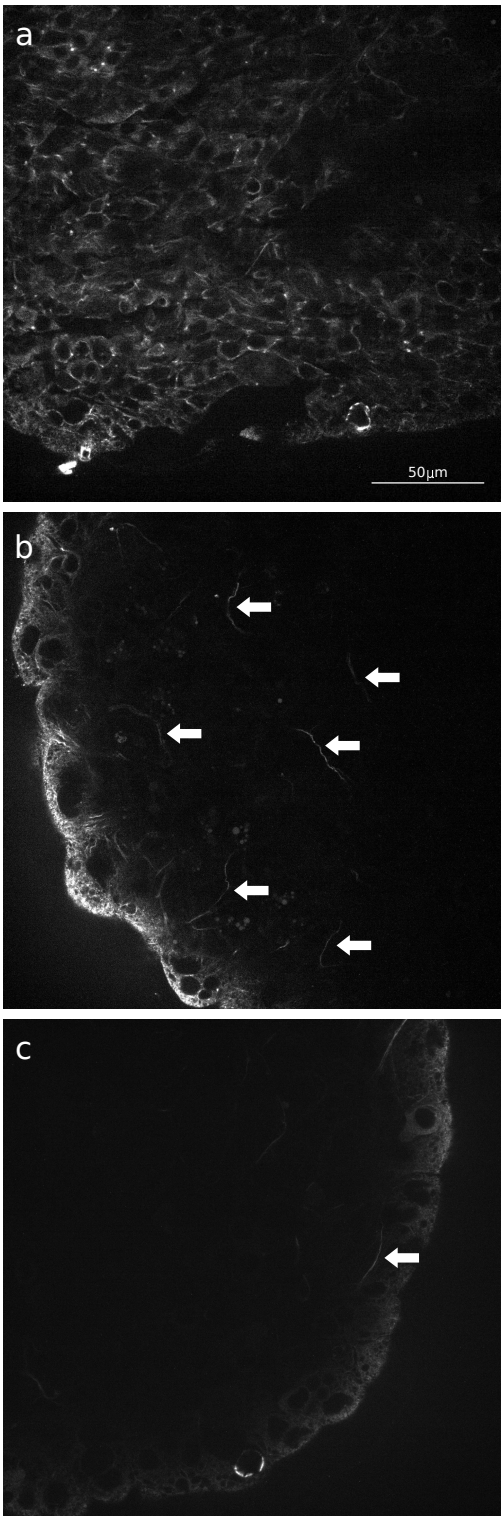

Fig. 8 Spheroids stained for microtubules. The aggregates were fixed, stained for microtubules and observed under the confocal microscope. **(a) Control**, stained after 24h after spheroid formation. **(b) Paclitaxel** rescued spheroids, stained 24h after paclitaxel treatment: there are polymerised microtubules, which appeared as supracellular structures (arrows) that were about 50μm long; however, there was less polymerised tubulin than in the control (a). **(c) Nocodazole**-treated *hydra* spheroids, stained simultaneously with (b): no polymerised microtubules were seen, except for one supracellular structure (arrow). The images are at the same scale; scale bar in (a)

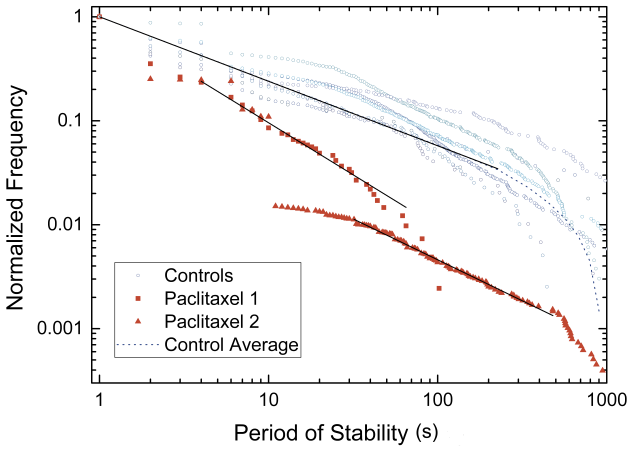

Fig. 9 Frequency (or probability) of occurrence of a fluctuation above the threshold as a function of the inter-fluctuation time interval. The control was approximated by a power law of $y = c \cdot x^{-\beta}$ with $\beta = 0.62 \pm 0.003$. Treatment with the microtubule-stabilising drug paclitaxel shifted the distribution to lower values. The exponents remained comparable: $\beta = 1.00 \pm 0.02$ and 0.79 ± 0.01, for the two paclitaxel cases.

sis under Experimental procedures section for details). A log-log plot reveals that paclitaxel-treated (stabilised microtubules) regeneration had a similar tendency to a power law as the control; however, this occurred with reduced absolute probabilities (Fig. 9). This indicates that paclitaxel increases the likelihood of shape fluctuations, in good agreement with figure 6.

Fourier transform of the volume (Fig. 1 a, centre) revealed $1/f$ scaling behaviour of the frequency spectrum, $1/f^{\alpha}$, where $\alpha = 1.43 \pm 0.21$ ($n = 8$) for control, above frequencies of 0.01Hz (Supplementary Information figure S5). Upon addition of nocodazole the amplitude was reduced by a factor of 10, but the $1/f$ scaling remained . The mean exponent in *hydra* treated with nocodazole was 0.84 ± 0.12 ($n = 9$ regenerations).

3 Discussion

Hydra tissue fragments tend to fold in to eventually form hollow spheroids made of a cell bilayer. For small spheroids that undergo *de-novo* axis formation, several transitions from a state of elongation in arbitrary directions to a state where the fluctuations followed a transient axis could be identified. Note that the latter case remains symmetric, as the situation was reversible (this corresponds to the usual definition of symmetry in physics). The abruptness of the last, irreversible transition to an increasingly elongated state not only correlated with the irreversible definition of axis positioning in space, but also with the changes in volume inflation. This behaviour shows mechanical synchronisation of the entire spheroid at the symmetry breaking instant, which suggests supracellular cytoskeletal organisation.

Freshly formed spheroids repeatedly inflate until they rupture, thereby losing cells. On theoretical grounds, osmotic inflation and tissue rupture have been suggested to be the driving forces for the resulting sawtooth oscillations in the volume [40], which is in good agreement with experimental findings. A dependence of the time span required for regeneration on the initial size of the spheroids was reported previously [1,21,41]. In the present study, the timespan correlated with the time needed to decrease the size of a spheroid, until a characteristic size was reached (Fig. 1). The impact of osmosis scales as the surface/volume (d^2/d^3, where d is the diameter), which means that smaller spheroids inflate relatively faster, and this could be a way to sense the size of a spheroid. However, the time required for artificial stem-cell clusters to polarise without external cues [42] also depends on the tissue size, which indicates that there might well be other mechanisms involved here.

Within the inflation and rupture sawtooth oscillations, we identified fluctuations at a shorter time scale (Fig. 1, right) that hinted at active contraction and/or controlled relaxation against the osmotically inflating spheroid. Spectral analysis by Fourier transform showed scale-free behaviour that followed $1/f^{\alpha}$ scaling (Supplementary Information figure S5).

The distribution of time intervals of the axis directional fluctuations (Fig. 9) agree well with a power law description. Soriano *et al.* observed *ks1* gene mRNA expression patterns that became scale free, that is, obeying a power law description at the moment of symmetry breaking [17]. A self-organised, critical [43], nearest-neighbour-coupled, lattice-based model quantitatively reproduced the scale-free distribution of *ks1* expression patterns as well as the axis orientation in a temperature gradient. The model was robust to the choice of its sole free parameter, the information exchange probability between neighboring, overcritically excited cells, fixed to about 0.95 [18]. Critical behaviour is observed in many complex, dissipating systems [44], in particular in the biological context [45].

Exact critical states are identified by power law behaviour and infinite sensitivity to external perturbations at the same time. However, although *hydra* has certain elements of a critical state, due to its finiteness and the statistically complex nature of the cells, an exact critical state cannot be reached. Therefore, these micropipette experiments (Fig. 2) still support the idea of mechanosensitivity of the symmetry-breaking process. In particular the location of the emerging heads corresponds to the molecular picture that we suggest below.

The slightly larger tissue fragments that formed spheroids that remained polarised throughout the regeneration process maintained their initial actin organisation (Fig. 4). This is in good agreement with [29], who showed that the supercellular orientation of actin fibres provided the direction for the body axis in larger aggregates. However, here we considered smaller aggregates than in [29]. We found that the large contractile actin structures known as myonemes (Fig. 3) and intracellular actin structures (Fig. 4) disappeared before symmetry breaking. Cortical actin, however, remained even during symmetry breaking, and may still contribute to a mechanotransduction process. Moreover, actin-fibre-modifying drugs accelerated the symmetry breaking process (see below).

Fibroblasts treated with the ROCK inhibitor Y-27632 showed reduced myosin light chain phosphorylation and increased two-dimensional spreading areas, with reduced levels of stress fibres at the cell centre. This was accompanied by increased actin concentration at the periphery; however, the line tension was decreased simultaneously [46]. Similar actions in *hydra* cells relate

very well to the observed changes in inflation patterns. For Y-27632-treated spheroids, symmetry breaking occurred substantially earlier compared to the control (Fig. 5). In general, decreased actin stress fibre levels reduce integrin-mediated cell adhesion. This decreased cell adhesion agrees well with the increased tendency to rupture, which leads to the observed diminished amplitude (and increased frequency) of the sawtooth inflation-relaxation patterns. In conjunction with the reduced contractility of the cell periphery, the increased surface area of Y-27632-treated spheroids matched well the overshoots during relaxation (Fig. 5, red circle) of the spheroid volume: As the spheroid breaks up due to osmotic inflation, there is a strong overshoot to low volumes that quickly disappears, which is again a sign of increased cell surface area. The symmetry breaking event occurs much earlier than in the control. We attribute this acceleration to the initial loss of polarity-defining actin structures in excellent agreement with[29].

SMIFH2 is a Formin homology 2 domain inhibitor, although its precise mode of action remains poorly understood[47]. Nevertheless in *in-vitro* studies, SMIFH2 diminished f-actin levels during the first hour(s) of application in different cell types. Subsequently, the entire cytoskeleton is reorganised, although with a notably different structure. Our observations in these regenerating *hydra* reflect this type of behaviour: initially there was no osmotic inflation, as a likely consequence of the loss of f-actin and the resulting weak cell adhesion. Oscillations were rescued after about 4h, which we interpret by the reappearance of f-actin. The volume then reaches a maximum compared to the control in terms of amplitude and time of occurrence. Again, the symmetry-breaking event occurs much earlier than in the control, which, again, is in good agreement with the initial loss of polarity-defining actin structures.

Phalloidin stabilises actin fibres, to prevent the reorganisation of the actin cytoskeleton. Accordingly the sawtooth oscillations observed here were of low amplitude (Fig. 5). A high oscillation frequency with low amplitude from the beginning of the inflation process indicates either frequent pressure release or residual contractility. Phalloidin-treated spheroids rounded up, which indicated the loss of any residual asymmetry in the shape, until they eventually disintegrated after 2 days.

Although in the present study the spheroids showed complex, well-defined patterns of motion, it appears that altering this pattern through the use of actin-modifying drugs does not necessarily prevent the axis-defining process. Treatment with actin stress fibre removing drugs even accelerated the symmetry breaking in agreement with[29]. The actin stabilizing drug phalloidin prevented symmetry breaking.

In traction-force rheological experiments on fibroblasts that were unspecifically glued to opposing surfaces, neither the microtubule-modifying drug nocodazole nor taxol had any noticeable influences on the mechanical responses of the cells to deformation[48]. In contrast, an actin-modifying drug resulted in large changes. Although microtubules do not directly contribute to the production of cytoskeletal forces, they are well known to orchestrate cell mechanics in a biological setting, via biochemical pathways. In particular, depolymerisation of microtubules stimulates cell contraction via Rho, through activation of the actin cytoskeleton, which results in stimulation of cell adhesion ([49] and references therein). Accordingly, we showed here that the nocodazole-treated *hydra* spheroids inflated more slowly compared to the control, and reached their maximum volumes only after as long as 36h (*i.e.*, compared to 6h for the control). This behaviour is well explained by a more contractile actin cytoskeleton that yields more slowly against the osmotic inflation pressure than in the control. The volume of nocodazole-treated spheroids increased more on a relative scale (Fig. 6). This can be understood in terms of the highly contracted and therefore smaller spheroids used as the starting point. At the same time, the increased cell adhesion that comes with increased contraction[50] prevents rupture, so that the volume can be inflated more before rupture occurs. Nocodazole prevented *hydra* symmetry breaking and regeneration (Fig. 6), while high doses of paclitaxel did not.

We observed that the microtubule-stabilising paclitaxel accelerated the rhythm of the high-frequency oscillations (Figs. 6 and 9). On the timescale of hours, paclitaxel has been shown to completely inhibit catecholamine release, thereby increasing cytoplasmic free Ca^{++} [51,52]. In *Hydra attenuata* catecholamine inhibitors could prevent regeneration. Dopamine is a specific catecholamine where the inhibition induces morphogenetic anomalies in gastral spheroids, which do not retain their natural organiser[53]. However, when paclitaxel was applied, no morphological anomalies were observed in any of the surviving spheroids in the present study, so this precise mechanism appears not to be important in our case. However, the activity of K^+ channels is determined by cytoskeletal interactions[54]. Even without superordinate neurological structures, the observed high frequency oscillations on top of the sawtooth oscillations may in principle result from interdependent effects of the cytoskeleton under osmotic tension in conjunction with cellular electrophysiology.

Paclitaxel increased the amplitudes of the sawtooth volume oscillations. This would require either increased adhesion within the tissue, or more likely, reduced cell contractility. The presence of microtubules is well known to reduce cell contraction and adhesion, via integrins controlled by Rho. In the presence of paclitaxel, the symmetry breaking event occurred earlier (around 10 h, instead of 18 h for the control), which again is well explained by the lower levels of actin stress fibres that comes with the stabilised microtubules. Nocodazole above 0.1 μM prevented *hydra* regeneration (Fig. 6); however, application of microtubule stabilising paclitaxel can rescue the process (Fig. 7). The amount of paclitaxel required to rescue nocodazole-treated spheroids correlated with the increased appearance of microtubular structures before symmetry breaking as observed under fluorescence microscopy (Fig. 8). In the absence of actin, microtubules are the only macroscopic polar filaments. The experiments suggest that they are functionally linked to axis establishment and symmetry breaking.

In adult *hydra*, cells elongate in the direction of the microtubules, while they contract in the perpendicular plane[55]. If the tissue is stretched by external forces, the microtubules will tend to orient in parallel to the stretch. This will promote further outgrowth and deformation towards a cylindrical shape during *hydra*

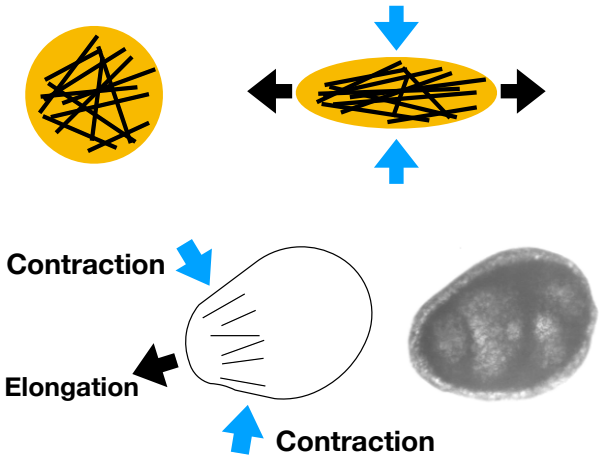

Fig. 10 *Hydra* cell shape and microtubules In adult *hydra*, microtubule alignment follows cell elongation in the microtubular direction[55]. **Top:** As a cell (left) is stretched, the filaments (black straight lines) will tend to align in the direction of the stretch (right). **Bottom:** This mechanism is expected to cause bulging (left), as observed during osmotic inflation of non-polarised hydra spheroids (right).

spheroid inflation, thereby stabilising elongated shapes. Indeed this type of deformation is observed (Fig. 10).

The current knowledge concerning the relevant Wnt molecular pathways and the cytoskeleton are illustrated in Fig. 11.

The canonical Wnt pathways involve nuclear translocation of β-catenin, which in turn enables the affected group of cells to change their fate, and to differentiate into a head organiser. During *hydra* axis-formation, increasing β-catenin nuclear translocation appears to be a natural way to slowly increase the head-forming potential as suggested by[18]. In the absence of dishevelled, a dynein – β-catenin complex can be expected to form in the cell cortex that can then tether the microtubules[65]. If the latter extend from the cell nucleus to the cell periphery at a sufficiently high concentration, the flux of β-catenin into the nucleus can be expected to increase. A sufficient (overcritical) increase here would enable a fraction of β-catenin to escape from degradation in the cytosol before reaching the nucleous.

Note that the ideas developed above agree well with the experiments where a micropipette exerted force on the spheroid. The head indeed appears within the annulus where the tissue must be stretched most so that cells are elongated in one direction because of the suction.

Our hypothesis also agrees well with previous studies in different model systems. Microtubules are involved in the polarisation of individual cells upon varied stimuli[66]. Brunet *et al.* showed mechanosensitive induction of nuclear translocation of β-catenin in zebrafish[30]. This induction can be directly activated by mechanical stimuli, and it leads to mesodermal invagination without prior Wnt activation. With the inhibition of microtubule polymerisation using nocodazole, as well as inhibition of myosin II using blebbistatin, β-catenin-dependent mesodermal invagination is suppressed[30]. Microtubules are involved in the asymmetric transport of Wnt8 mRNA during induction of the embryonic axis in zebrafish[67]. Non-canonical Wnt signalling and β-catenin signalling are involved in osteogenic differentiation upon oscillatory mechanical stimulus[68]. The importance of microtubules in the establishment of embryonic polarity has also been shown in *C. elegans*[69]. Kwan *et al.* showed that in *Xenopus*, a sufficient mass of polymerised microtubules is necessary for convergent extension during embryonic development[70].

4 Conclusions

Symmetry breaking in *hydra* spheroids of around 10,000 cells exhibits coordinated mechanical fluctuations and oscillations. Here, we have shown that these spheroids show a clear and abrupt transition to an oblong shape, from where on the position of the related axis remains irreversibly defined. Cytosolic actin fibres disappear before axis definition, and their removal by actin-modifying drugs accelerated the symmetry-breaking process. This agrees well with larger tissue fragments, where the remaining actin fibres dictate the polarity of the regenerating *hydra*[29]. We have presented strong evidence suggesting that polymerised microtubules are required for symmetry breaking. Remaining in excellent agreement with observations in other species, we formulate the hypothesis that microtubules are an important direction-defining molecular element that tends to align by mechanical coupling. We suspect that microtuble orientation can increase β-catenin nuclear translocation in conjunction with dynein[65], which eventually results in the differentiation of a head organiser. This could explain why the mechanical oscillations appear as a clock driving the process[21]. The mechanical connection through the extracellular matrix is a suitable means to enable collective dynamics and synchronisation of many cells over large distances, and in particular to enable the cells to polarise cooperatively on the entire spheroid. Since this process is based on fluctuations rather than clear molecular signatures, it is difficult to apprehend.

5 Experimental procedures

Hydra strains

The wildtype strain of *Hydra vulgaris* and the transgenic strains *Hydra magnipapillata* ks1 GFP, *Hydra vulgaris* 12ASAktin+GFP Ecto- and *Hydra vulgaris* 12ASAktin+GFP endodermal (all kindly provided by the Bosch group in Kiel, Germany) were used for experiments and imaging. Unless otherwise stated, the transgenic *Hydra magnipapillata* ks1-GFP were used for the experiments.

Preparation and culturing of *hydra*

Unless otherwise stated, all experiments with *hydra* were performed in Volvic mineral water (Danone Waters, Deutschland GmbH). *Hydra* were fed with artemia, but starved 24h prior to experiments. To obtain tissue pieces, a doughnut-like slice was cut from the centre of the body column. This slice was then cut into four equal pieces, which resulted in fragments that form spheroids of 0.18mm to 0.30mm in diameter. The technique follows the procedure described in[18].

Staining

Microtubules: *Hydra* balls were relaxed for 1min with 2% urethane in *hydra* medium, and fixed for 1h at room tempera-

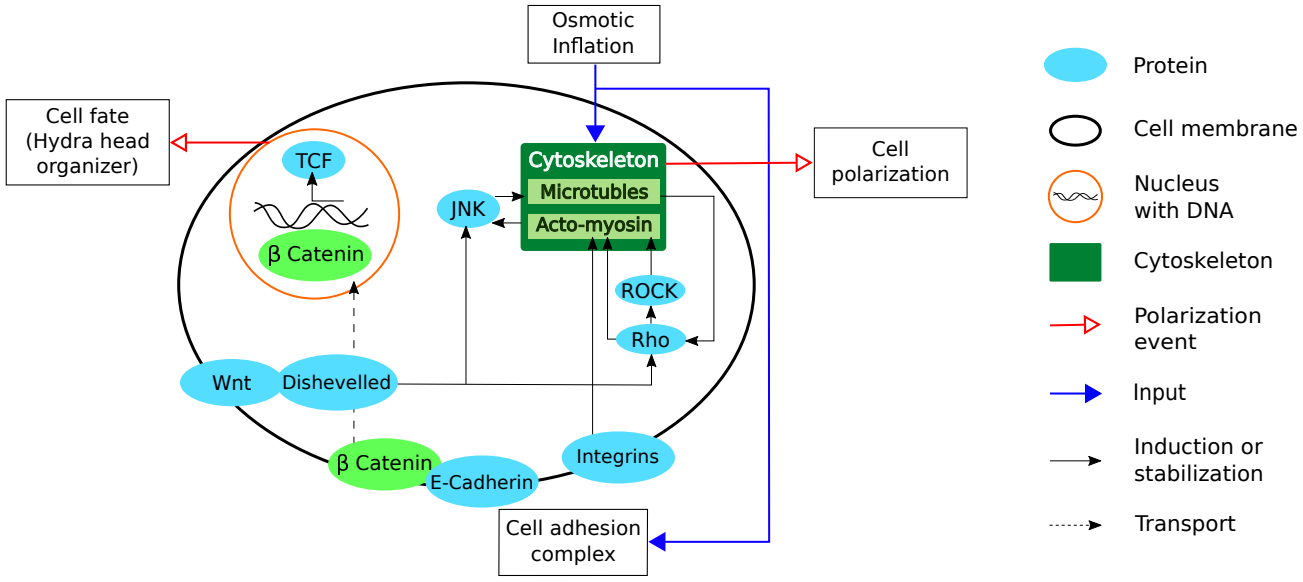

Fig. 11 Wnt pathways overlap with the biochemical reactions to mechanical stimulus. The dishevelled complex protects cytosolic β-catenin from degradation by the catenin degradation complex. β-catenin, which is located in particular at the intracellular side of E-cadherin, can then be translocated into the nucleus to activate the transcription of T-cell factor (TCF)[56]. TCF induces the formation of the head organiser in *hydra*[7,9]. In *Drosophila*[57] and *Zebrafish*[30], β-catenin induces mesodermal invagination, which leads to gastrulation. In turn, β-catenin nuclear translocation can induce Wnt expression[58]. Wnt controls acto-myosin contraction via Rho, including ROCK-dependent protein kinase[59]. The Wnt-dishevelled complex/ pathway can act locally to stabilise microtubules[60]. In addition, the Wnt-dishevelled complex can reorganise the microtubule cytoskeleton via JNK (c-Jun N terminal kinase, which is involved in cell polarisation)[61]. JNK-mediated cell polarisation can also be induced via mechanical stimuli[62], thus leading to mechanically induced cell polarisation. Wnt-controlled JNK activity mediates convergent extension during embryonic development[63,64]. Within this framework, we hypothesise that in conjunction with long, oriented microtubules, a β-catenin - dynein - microtubule complex[65] can increase the transport of β-catenin to the nucleus.

ture with Landowsky fixative (48% ethanol, 3.6% formaldehyde, 3.8% acetic acid, in water). After three washes with phosphate-buffered saline (PBS), they were permeabilised with 0.8% Triton X-100 in PBS for 15min, blocked with 0.1% Triton X-100, 1% BSA (w/v) in PBS for 20min, and incubated overnight with a monoclonal anti-tubulin antibody (clone 2-28-33; Sigma) at 4°C. Subsequently, these were washed three times with PBS and incubated for 2h with the anti-mouse IgG (whole molecule)-FITC secondary antibody (Sigma). Myonemes: Labelling of the myonemes was performed using rhodamine/ phalloidin, following the protocol above for the permeabilisation.

Micropipette aspiration

Micropipettes were pulled from borosilicate glass capillaries using a pipette puller (model P-97; Sutter Instruments). The glass capillaries had an outer diameter of 1mm and an inner diameter of 0.5mm. After pulling, the pipettes were trimmed to achieve blunt ends with an outer diameter of 200μm. For the *hydra* to tolerate the contact, the tips needed to be smoothed on the outside and inside of the opening, and the diameter needed to be as small as possible. A microforge was used for smoothing. The capillaries were connected to a homemade low-pressure system using a syringe installed on a screw thread and a U-shaped tube, with marks as a manometer to control the pressure.

The set-up was mounted onto a microscope (IX70; Olympus). To account for the sensitivity of the *hydra* to contaminants and to avoid evaporation, the capillary experiments were performed in closed glass Petri dishes with a hole in the lid for the micropipette. The *hydra* tissue was allowed to rest and heal for 30 min after cutting. The capillary tip was moved into close proximity with the *hydra* and held in the focus plane using a micromanipulator (Xeno Works; Sutter Instruments). After contact, the pressure within the pipette was quickly decreased to avoid escape. After stabilisation, the pressure was decreased to the lowest pressure necessary to secure the *hydra* in place. If necessary, adjustments in the positioning of the *hydra* were made to move it back into focus, using the micromanipulator.

Microscopy

Visualisation of the actin structures was performed using an inverted microscope (TI-Eclipse; Nikon), with a spinning head (Yokogawa CSU-W1; Andor), a combiner (LU-NV; Nikon), 70 mW, and a 4-million-pixel digital camera (ORCA Flash 4.0 V2 CMOS; Hamamatsu) controlled by NIS Elements software. For imaging actin, a 20x CFI-Plan Apo NA 0.75 objective with a working distance of 1.0 mm was used. The excitation/ emission wavelengths were 540/565 nm. A 60x oil immersion objective (Plan Apo; NA 1.4) was used to collect the images of the microtubules under excitation/emission wavelengths of 488/540 nm. The microscopy of the hydra spheroid regeneration patterns was performed using a phase contrast microscope (IX70; Olympus) equipped with a digital camera (G1-2000; Moravian Instruments). For the regeneration pattern analysis, the microscopy images were recorded at a frame rate of 1/s.

Sample preparation

For regeneration, the samples were prepared in culture medium, which was supplemented with drugs in some experiments. Drops of 30μl that included one spheroid each were pipetted onto the lid of a plastic petri dish (diameter, 5cm; Corning). The lids were put on top of medium-containing dishes, which were then sealed with parafilm to avoid evaporation. The *hydra* floated in the drops hanging down from the lids. Hanging drops allowed the fluctuations of the main axis orientation to be seen more clearly compared to the bottom of a petri dish. This also kept the tissue fragments in focus. Control experiments were performed using silica-bead particles. Confocal microscopy was performed in 35-mm diameter dishes (Ibidi μ). Imaging was performed with a PLN 10x (Olympus) objective with larger working distance, required by the use of the petri dishes.

Image analysis

Image series were transformed into binary images, and particle analysis was performed using the open-source FIJI Imaging software. Area, circularity, axis length and main axis orientation were determined. The data obtained this way were analysed and plotted using Origin Pro 8.6 (Origin Lab) and MatLab R2011b (Mathworks). Confocal images were processed using FIJI.

All of the correlation functions were calculated using Origin Pro 8.6. To analyse the correlations between volume and angle, and others, cross-correlation was performed over the regeneration from the beginning until the appearance of tentacles. Cross-correlation provides a measure of similarity between two series as a function of the lag of one series relative to the other. The following function was used for the discrete functions a and b:

$$(a \cdot b)[n] = \sum_{n=-\infty}^{\infty} f^*[m]g[m+n]$$

where f^* is the complex conjugate, and n is the lag. The correlations between the size changes and time until the final size of the spheroids were performed using Pearsons correlation coefficients. This coefficient represents a measure of the strength and direction of the linear relationship between two variables, and it is defined as the covariance of the variables divided by the product of their standard deviations. The correlations between the size changes and the time until mechanical symmetry breaking were performed using Spearman correlation coefficients. This coefficient represents a measure of the strength and direction of the monotonic relationship between two variables. Moreover, to analyse the fluctuating behaviour of the spheroids, the differences between two subsequent values of the angular position were calculated for all of the data points. To avoid artificially high angle differences that can result from angles that change between areas closer to 180 degrees compared to areas closer to 0 degrees, the mean scattering of the angle during the stable phases was measured and used as the threshold. If the anglular differences were within this threshold, the spheroid was considered to be stable. To further analyse these fluctuations, the period of time the spheroids remained in either stable or unstable states were measured and plotted against the level of appearance of a period of a given length.

Furthermore, spectral analysis of the inflation was performed by subtracting a linear fit from each individual inflation, with detrending of the data. Fast Fourier transform was performed to compute the amplitude spectra. According to the Nyquist-Shannon theorem, frequencies above 0.1 Hz were discarded.

Drugs

The drugs for the analyses depicted in figures 5 and 6 were used at the highest viable concentrations, which were determined on adult *hydra* prior to the experiments. Nocodazole (Sigma Aldrich) was used at a working concentration of 10^{-6} M, and stored at 6×10^{-3} M in dimethylsulphoxide (DMSO). Paclitaxel (Sigma Aldrich) was used at a working concentration of 10^{-6} M, and stored as a 10^{-3} M solution in DMSO. Y-27632 was used at a working concentration of 10^{-8}M, with the stock solution at 10^{-3} M in DMSO. SMIFH2 was used at a working concentration of $2.5{\cdot}10^{-5}$ M, which was stored in DMSO at 10^{-3} M. Phalloidin was used at a working concentration of $2 \cdot 10^{-5}$ M.

For experiments where the action of nocodazole was probed alongside paclitaxel, the *hydra* balls ($200-300\mu$m) were treated with a combination of nocodazole (1μM, 0.1μM, 0.01M) and paclitaxol (1μM, 0.1μM, 0.01μM) at different concentrations ($n = 30$). The minimal effective concentrations of nocodazole for inhibition of the regeneration was determined as 0.1μM ($n = 15$, out of 15). To suppress the effects of nocodazole, the minimum concentration of paclitaxel was determined as 0.1μM. In separate experiments, *hydra* balls ($n = 15$) were first incubated with nocodozole (0.1μM) for 24h, and then with paclitaxel (0.1μM) . We observed that the time to regenerate *hydra* if paclitaxel rescued the process, was prolonged significantly (by about 40h in nocodazole-supplemented medium), compared to untreated controls. However, the hydra spheroids survived and regenerated ($n = 14$, out of 15).

6 Author Contributions

H.D. and A.O conceived of the study, interpreted the data and drafted the manuscript. Regeneration experiments and analysis were performed by H.D., A.P. and V.G.. Rhodamine-phalloidin staining was performed by M.S. and H.D. Microtubule staining was perfomed by A.P. Confocal microscopy was performed by E.T.. Analytical guidance was provided by M.S, V.G. and A.O.. F.L. and A.O. supervised.

7 Acknowledgements

We acknowledge support by Heiko Rieger in connection with the interpretation of the spectral analysis data. Funding was provided by Saarland University and Deutsche Forschungsgemeinschaft, Collaborative Research Centre (SFB) 1027. The transgenic actin-GFP *hydra* were kindly provided by the Bosch Laboratory.

References

1 A. Gierer, S. Berking, H. Bode, C. N. David, K. Flick, G. Hansmann, H. Schaller and E. Trenkner, *Nature New Biology*, 1972, **239**, 98–101.

2 H. R. Bode, *Cold Spring Harbor Perspectives in Biology*, 2009, **1**, a000463.

3 A. Gierer, *International Journal of Developmental Biology*, 2012, **56**, 437–445.

4 S. Wennekamp, S. Mesecke, F. Nédélec and T. Hiiragi, *Nature Reviews Molecular Cell Biology*, 2013, **14**, 452–459.

5 C. Guder, S. Pinho, T. G. Nacak, H. A. Schmidt, B. Hobmayer, C. Niehrs and T. W. Holstein, *Development*, 2006, **133**, 901–911.

6 M. Broun, L. Gee, B. Reinhardt and H. R. Bode, *Development*, 2005, **132**, 2907–2916.

7 H. Bode, *Annual Review of Genetics*, 2011, **45**, 105–117.

8 H. R. Bode, *International Journal of Developmental Biology*, 2012, **56**, 473–478.

9 G. Plickert, V. Jacoby, U. Frank, W. A. Müller and O. Mokady, *Developmental Biology*, 2006, **298**, 368–378.

10 B. Hobmayer, F. Rentzsch, K. Kuhn, C. M. Happel, C. C. von Laue, P. Snyder, U. Rothbächer and T. W. Holstein, *Nature*, 2000, **407**, 186–189.

11 T. Lengfeld, H. Watanabe, O. Simakov, D. Lindgens, L. Gee, L. Law, H. A. Schmidt, S. Özbek, H. Bode and T. W. Holstein, *Developmental Biology*, 2009, **330**, 186–199.

12 R. Augustin, A. Franke, K. Khalturin, R. Kiko, S. Siebert, G. Hemmrich and T. C. G. Bosch, *Developmental Biology*, 2006, **296**, 62–70.

13 J.-R. Huynh and D. St Johnston, *Current Biology*, 2004, **14**, R438–R449.

14 A. Castro-e Silva and A. T. Bernardes, *Physica A: Statistical Mechanics and its Applications*, 2005, **352**, 535–546.

15 U. Technau, C. C. von Laue, F. Rentzsch, S. Luft, B. Hobmayer, H. R. Bode and T. W. Holstein, *Proceedings of the National Academy of Sciences*, 2000, **97**, 12127–12131.

16 R. Weinziger, L. M. Salgado, C. N. David and T. Bosch, *Development*, 1994, **120**, 2511–2517.

17 J. Soriano, C. Colombo and A. Ott, *Physical Review Letters*, 2006, **97**, 258102.

18 A. Gamba, M. Nicodemi, J. Soriano and A. Ott, *Physical Review Letters*, 2012, **108**, 158103.

19 H. Meinhardt, *International Journal of Developmental Biology*, 2012, **56**, 447–462.

20 C. Fütterer, C. Colombo, F. Jülicher and A. Ott, *EPL (Europhysics Letters)*, 2003, **64**, 137–143.

21 J. Soriano, S. Rüdiger, P. Pullarkat and A. Ott, *Biophysical Journal*, 2009, **96**, 1649–1660.

22 M. Mercker, D. Hartmann and A. Marciniak-Czochra, *PLOS ONE*, 2013, **8**, e82617.

23 L. V. Beloussov and V. I. Grabovsky, *International Journal of Developmental Biology*, 2006, **50**, 81–92.

24 B. Wickstead and K. Gull, *The Journal of Cell Biology*, 2011, **194**, 513–525.

25 M. Pilhofer, M. S. Ladinsky, A. W. McDowall, G. Petroni and G. J. Jensen, *PLOS Biology*, 2011, **9**, e1001213.

26 R. O. Hynes, *The Journal of Cell Biology*, 2012, **196**, 671–679.

27 S. Özbek, P. G. Balasubramanian, R. Chiquet-Ehrismann, R. P. Tucker and J. C. Adams, *Molecular Biology of the Cell*, 2010, **21**, 4300–4305.

28 D. L. West, *Tissue and Cell*, 1978, **10**, 629–646.

29 A. Livshits, L. Shani-Zerbib, Y. Maroudas-Sacks, E. Braun and K. Keren, *Cell Reports*, 2017, **18**, 1410–1421.

30 T. Brunet, A. Bouclet, P. Ahmadi, D. Mitrossilis, B. Driquez, A.-C. Brunet, L. Henry, F. Serman, G. Béalle, C. Ménager, F. Dumas-Bouchiat, D. Givord, C. Yanicostas, D. Le-Roy, N. M. Dempsey, A. Plessis and E. Farge, *Nature Communications*, 2013, **4**, 2821.

31 L. He, X. Wang, H. L. Tang and D. J. Montell, *Nature Cell Biology*, 2010, **12**, 1133–1142.

32 C. Gally, F. Wissler, H. Zahreddine, S. Quintin, F. Landmann and M. Labouesse, *Development*, 2009, **136**, 3109–3119.

33 E. Farge, *Current Topics in Developmental Biology*, Academic Press, 2011, vol. 95, pp. 243–265.

34 S. Piccolo, *Nature*, 2013, **504**, 223–225.

35 *Forces and Tension in Development*, ed. M. Labouesse, Academic Press, 2011, vol. 95.

36 R. Fickentscher, P. Struntz and M. Weiss, *Physical Review Letters*, 2016, **117**, 188101.

37 J. Negrete Jr, A. Pumir, H.-F. Hsu, C. Westendorf, M. Tarantola, C. Beta and E. Bodenschatz, *Physical Review Letters*, 2016, **117**, 148102.

38 S. Narumiya, T. Ishizaki and M. Ufhata, *Methods in Enzymology*, Academic Press, 2000, vol. 325, pp. 273–284.

39 S. A. Rizvi, E. M. Neidt, J. Cui, Z. Feiger, C. T. Skau, M. L. Gardel, S. A. Kozmin and D. R. Kovar, *Chemistry & Biology*, 2009, **16**, 1158–1168.

40 M. Kücken, J. Soriano, P. A. Pullarkat, A. Ott and E. M. Nicola, *Biophysical Journal*, 2008, **95**, 978–985.

41 H. Shimizu, Y. Sawada and T. Sugiyama, *Developmental Biology*, 1993, **155**, 287–296.

42 S. C. van den Brink, P. Baillie-Johnson, T. Balayo, A.-K. Hadjantonakis, S. Nowotschin, D. A. Turner and A. M. Arias, *Development*, 2014, **141**, 4231–4242.

43 P. Bak, C. Tang and K. Wiesenfeld, *Physical Review Letters*, 1987, **59**, 381–384.

44 M. F. Shlesinger, *Annals of the New York Academy of Sciences*, 1987, **504**, 214–228.

45 T. Mora and W. Bialek, *Journal of Statistical Physics*, 2011, **144**, 268–302.

46 C. Labouesse, A. B. Verkhovsky, J.-J. Meister, C. Gabella and B. Vianay, *Biophysical Journal*, 2015, **108**, 2437–2447.

47 T. Isogai, R. Van Der Kammen and M. Innocenti, *Scientific Reports*, 2015, **5**, 9802.

48 O. Thoumine and A. Ott, *Journal of Cell Science*, 1997, **110**, 2109–2116.

49 S. Etienne-Manneville, *Traffic*, 2004, **5**, 470–477.

50 S. Safran, N. Gov, A. Nicolas, U. Schwarz and T. Tlusty, *Physica A: Statistical Mechanics and its Applications*, 2005, **352**, 171–201.

51 J. Thuret-Carnahan, J.-L. Bossu, A. Feltz, K. Langley and D. Aunis, *The Journal of Cell Biology*, 1985, **100**, 1863–1874.

52 J. T. Smyth, W. I. DeHaven, G. S. Bird and J. W. Putney, *Journal of Cell Science*, 2007, **120**, 3762–3771.

53 T. Ostroumova and L. Markova, *Neuroscience and Behavioral Physiology*, 2002, **32**, 293–298.

54 J. Camacho, A. Sánchez, W. Stühmer and L. A. Pardo, *Pflügers Archiv*, 2000, **441**, 167–174.

55 Y. Takaku, H. Shimizu and T. Fujisawa, *Developmental Biology*, 2011, **350**, 228–237.

56 C. Y. Logan and R. Nusse, *Annual Review of Cell and Developmental Biology*, 2004, **20**, 781–810.

57 R. Nusse and H. Varmus, *The EMBO Journal*, 2012, **31**, 2670–2684.

58 Y. Nakamura, C. D. Tsiairis, S. Özbek and T. W. Holstein, *Proceedings of the National Academy of Sciences*, 2011, **108**, 9137–9142.

59 K. Schlessinger, A. Hall and N. Tolwinski, *Genes & Development*, 2009, **23**, 265–277.

60 L. Ciani, O. Krylova, M. J. Smalley, T. C. Dale and P. C. Salinas, *The Journal of Cell Biology*, 2004, **164**, 243–253.

61 L. Ciani and P. C. Salinas, *BMC Cell Biology*, 2007, **8**, 27.

62 R. Kaunas, S. Usami and S. Chien, *Cellular Signalling*, 2006, **18**, 1924–1931.

63 S. Sokol, *Nature Cell Biology*, 2000, **2**, E124–E125.

64 H. Yamanaka, T. Moriguchi, N. Masuyama, M. Kusakabe, H. Hanafusa, R. Takada, S. Takada and E. Nishida, *EMBO Reports*, 2002, **3**, 69–75.

65 L. A. Ligon, S. Karki, M. Tokito and E. L. Holzbaur, *Nature Cell Biology*, 2001, **3**, 913.

66 G. G. Gundersen, E. R. Gomes and Y. Wen, *Current Opinion in Cell Biology*, 2004, **16**, 106–112.

67 X. Ge, D. Grotjahn, E. Welch, J. Lyman-Gingerich, C. Holguin, E. Dimitrova, E. W. Abrams, T. Gupta, F. L. Marlow, T. Yabe, A. Adler, M. C. Mullins and F. Pelegri, *PLOS Genetics*, 2014, **10**, e1004422.

68 E. J. Arnsdorf, P. Tummala and C. R. Jacobs, *PLOS ONE*, 2009, **4**, e5388.

69 B. Goldstein, *Current Biology*, 2000, **10**, R820–R822.

70 K. M. Kwan and M. W. Kirschner, *Development*, 2005, **132**, 4599–4610.